

- supervised approach-and-retract cycles (10) in SWT containing different concentrations of  $\text{Ca}^{2+}$  and  $\text{Mg}^{2+}$ .
- Approach-and-retract cycles are sometimes called force distance curves or force plots. While the cantilever deflection was permanently monitored, the tip was slowly moved (0.1 Hz) toward the substrate until contact and was then retracted. The hysteresis is a direct measure of the adhesion force. The stiffness of the cantilevers (Park Scientific Instruments, Mountain View, CA) was verified within 30% by taking approach-and-retract cycles on top of three different Si levers that had been individually calibrated by the manufacturer.
  - For steric and statistical reasons, the approach-and-retract cycles did not always result in an adhesion peak. The frequency is a measure of interaction probabilities.
  - D. J. Rice and T. Humphreys, *J. Biol. Chem.* **258**, 6394 (1983).
  - This length assumes that the g200 acidic glycan had the extended structure of a hyaluronate polyanion [W. T. Winter and S. Arnott, *J. Mol. Biol.* **117**, 761 (1977)].
  - A Lennard-Jones (12-6) potential has two free parameters that can be adjusted with respect to the experimental parameters: binding energy (348 kJ/mol) and binding length (0.154 nm). For an individual C-C bond, the gradient of the potential is the negative force and the calculated maximum is the rupture force.
  - The Archimedes force,  $gV(\rho_{\text{cell}} - \rho_{\text{buffer}})$ , equals 0.15 to 0.35 pN, where  $g$  is the acceleration due to gravity (9.81 N/kg),  $V$  is the volume of a cell (for example, a sphere 10  $\mu\text{m}$  in diameter),  $\rho_{\text{cell}}$  is the density of a cell [measured as in C. Gutierrez *et al.*, *J. Immunol. Methods* **29**, 57 (1979)], and  $\rho_{\text{buffer}}$  is the density of seawater (1020  $\text{kg}/\text{m}^3$ ).
  - We selected imaging of physisorbed rather than covalently attached APs because (i) on a nonfunc-

tionalized mica substrate the polysaccharide AP arms are also attached to the surface, and (ii) the smoothness of the mica facilitated imaging of the very fine AP arms. For the EM images, the mica was charged by incubation in 3-aminopropyltriethoxysilane (APTS) (Fluka) for 4 min at room temperature. Images are similar to those in S. Humphreys, T. Humphreys, J. Sano, *J. Supramol. Struct.* **7**, 339 (1977).

17. We thank D. Hartman, Z. Markovic, and G. De Libero for helpful discussions and critical reading of this manuscript, M. Dreier and M. Hegner for useful comments, E. Paris for technical assistance, and M. Häner for the EM imaging. Supported by Swiss National Science Foundation grants 2000-037496.93 (to H.-J.G.), 3100-037733.93, and 3100-039721.93 (to G.N.M.), and Cancer League Basel grant 5354 (to G.N.M.).

11 October 1994; accepted 20 December 1994

## A Regulatory Role for ARF6 in Receptor-Mediated Endocytosis

Crislyn D'Souza-Schorey, Guangpu Li, Maria I. Colombo, Philip D. Stahl\*

Adenosine diphosphate-ribosylation factor 6 (ARF6), ARF6 mutants, and ARF1 were transiently expressed in Chinese hamster ovary cells, and the effects on receptor-mediated endocytosis were assessed. Overexpressed ARF6 localized to the cell periphery and led to a redistribution of transferrin receptors to the cell surface and a decrease in the rate of uptake of transferrin. Similar results were obtained when a mutant defective in guanosine triphosphate hydrolysis was expressed. Expression of a dominant negative mutant, ARF6(T27N), resulted in an intracellular distribution of transferrin receptors and an inhibition of transferrin recycling to the cell surface. In contrast, overexpression of ARF1 had little or no effect on these parameters of endocytosis.

Intracellular membrane trafficking involves a series of membrane budding and fusion events. These are regulated by specific cytosolic and membrane-associated protein factors, among which are a group of Ras-like small guanosine triphosphatases (GTPases) called adenosine diphosphate (ADP)-ribosylation factors (ARFs), originally identified as cofactors required for the cholera toxin-catalyzed ADP ribosylation of  $\text{G}\alpha_s$  (1). The ARF family consists of 15 structurally related gene products that include 6 ARF proteins and 11 ARF-like proteins (2). The ARF proteins are divided into three classes on the basis of size and amino acid identity. ARFs 1 to 3 (181 amino acids) form class I, ARFs 4 and 5 (180 amino acids) form class II, and ARF6 (175 amino acids) forms class III (3).

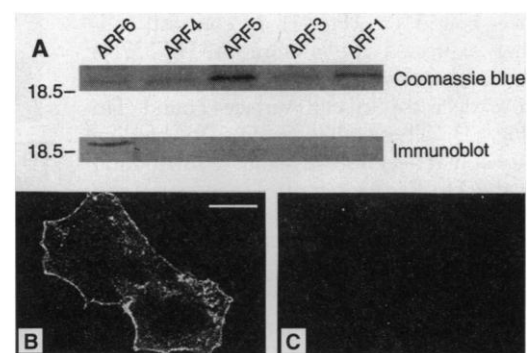
The best characterized ARF protein is ARF1. It is localized to the Golgi apparatus (4) and has a central role in intra-Golgi transport. It is involved in the recruitment of cytosolic coat proteins to Golgi membranes

during the formation of transport vesicles (5). The ARFs are also implicated in endoplasmic reticulum to Golgi transport (6), nuclear vesicle fusion (7), and endosome fusion (8). In these cases, however, the specific ARFs involved and their molecular

mechanisms of action are less clear. Here, we demonstrate that ARF6 is localized to the cell periphery and that overexpression of ARF6 or ARF6 mutants (but not ARF1) causes dramatic alterations in endocytic traffic.

Our studies were carried out in a Chinese hamster ovary cell line that overexpresses the human transferrin receptor (TRVb-1) (9). We transiently expressed ARF6 by using Sindbis virus as an expression vector (10). To monitor the expression of ARF6 and to determine its intracellular distribution, rabbit antiserum to ARF6 was raised against a peptide corresponding to the COOH-terminal region of the protein. This antiserum reacted specifically with ARF6, and no cross reaction was observed with any of the other ARF proteins tested, including ARF1, ARF3, ARF4, and ARF5, as shown by protein immunoblot analysis (Fig. 1). The antibody was used to localize ARF6 by confocal immunofluorescence microscopy in TRVb-1 cells overexpressing ARF6. The overexpressed protein exhibited a peripheral distri-

**Fig. 1.** (A) Specificity of the ARF6 antibody. BL21(DE3) bacteria coexpressing ARF proteins and *N*-myristoyltransferase were grown in 2 ml of Luria broth to an absorbance at 600 nm of 0.8 and were then induced with isopropyl- $\beta$ -D-thiogalactopyranoside for 2 hours. The cell pellet was resuspended in SDS sample buffer, boiled for 5 min, and centrifuged at high speed. Aliquots of the supernatant were run on 12% SDS gels. The SDS gel proteins were visualized by Coomassie blue staining or were transferred to nitrocellulose membranes and blotted with an ARF6 antibody (23). Size markers are indicated on the left in kilodaltons. (B and C) Localization of ARF6 by confocal immunofluorescence microscopy. TRVb-1 cells grown on cover slips were infected with recombinant virus expressing ARF6 (24). At 5 hours after infection, cover slips were fixed with 2% formaldehyde (freshly diluted with PBS) for 15 min, quenched, and permeabilized with PBS containing 0.1 M  $\text{NH}_4\text{Cl}$ , 0.2% gelatin, and 0.05% Triton X-100. Incubation with the affinity-purified ARF6 antibody (B) or immunoglobulin G (IgG) fraction from the preimmune serum (C) was conducted at room temperature for 2 hours. The secondary antibody was a goat antibody to rabbit IgG coupled to fluorescein isothiocyanate (FITC). The cover slips were mounted in 1% propyl gallate and viewed with a Zeiss axiovert microscope and a Bio-Rad confocal scanning imaging system. Bar = 10  $\mu\text{m}$ .



Department of Cell Biology and Physiology, Washington University School of Medicine, 660 South Euclid, Box 8226, St. Louis, MO 63110, USA.

\*To whom correspondence should be addressed.

bution localizing mainly to the plasma membrane and some apparently internal punctate structures.

In addition to ARF6, two ARF6 mutants (T27N and Q67L, where Thr<sup>27</sup> → Asn and Gln<sup>67</sup> → Leu, respectively) as well as ARF1 were also transiently expressed in TRVb-1 cells. The expression of ARF6 and its mutant derivatives at 5 hours after infection was detected by protein immunoblot analysis (Fig. 2). Levels of ARF1 expression were at least 10-fold over those of the background (11). By analogy to other well-characterized Ras-like small GTPases, including ARF1, mutant ARF6(T27N) was expected to be defective in GTP binding and ARF6(Q67L) was expected to be defective in GTP hydrolysis. To confirm this point, we analyzed cell lysates containing overexpressed ARF6, ARF6(T27N), and ARF6(Q67L) for their ability to bind [ $\alpha$ -<sup>32</sup>P]GTP. As shown in Fig. 2, ARF6 and ARF6(Q67L) bound [ $\alpha$ -<sup>32</sup>P]GTP, whereas ARF6(T27N) exhibited only background levels of [ $\alpha$ -<sup>32</sup>P]GTP binding. Thus, the predicted guanine nucleotide binding phenotype of other Ras-related GTPases was also applicable to ARF6.

The peripheral distribution of ARF6 prompted us to test whether ARF6 could play a role in endocytic traffic. We monitored receptor-mediated endocytosis by following transferrin receptor (Tfn-R) recycling in TRVb-1 cells overexpressing ARF6, ARF6(T27N), ARF6(Q67L), and ARF1. First, we determined the steady-state Tfn-R distribution on the cell surface. Cells were incubated at 4°C with a saturating concentration of [<sup>125</sup>I]Tfn, and the amount of bound radioactivity was measured. Overexpression of ARF6 resulted in a significant increase in cell surface binding of Tfn as compared to that in control cells infected with the vector virus (Fig. 3). Like ARF6, the mutant ARF6(Q67L) that is defective in GTP hydrolysis also increased cell surface-bound Tfn (Fig. 3). In contrast, cells that expressed the mutant ARF6(T27N) that is defective in GTP binding showed a 70% decrease in cell surface-bound Tfn (Fig. 3). These changes in Tfn binding probably reflect a steady-state redistribution of the Tfn-Rs. As a control, overexpression of ARF1 had little effect on the cell surface distribution of Tfn-Rs (Fig. 3), indicating that the observed receptor redistribution was induced specifically by expression of ARF6 and its mutant derivatives. The alterations in cell surface Tfn-R distribution after overexpression of ARF6 or ARF6 mutants was confirmed by confocal immunofluorescence microscopy (Fig. 3). A uniformly dispersed punctate pattern characteristic of Tfn-Rs was observed in control cells infected with the vector virus, whereas in cells overexpressing ARF6 and ARF6(Q67L) a redistribution of the recep-

tors to the plasma membrane was observed (Fig. 3). Consistent with results obtained from cell surface-binding studies, cells

overexpressing ARF6(T27N) exhibited little staining at the plasma membrane compared to the prominent fluorescent staining of in-

**Fig. 2. (A)** Expression of ARF6 and ARF6 mutants in TRVb-1 cells. TRVb-1 cell monolayers in 35-mm dishes ( $5 \times 10^5$  cells per dish) were infected with either the vector virus as a negative control or with recombinant Sindbis viruses capable of expressing ARF6, ARF6(Q67L), and ARF6(T27N) (24). At 5 hours after infection, the cell monolayers were rinsed once with PBS and lysed with 1% SDS (200  $\mu$ l per dish). Aliquots of the cell lysates were then analyzed by SDS-polyacrylamide gel electrophoresis (12% gel). SDS gel proteins were transferred to a nitrocellulose membrane, and ARF6 expression was detected by immunoblot analysis with the use of an ARF6-specific rabbit antiserum (23). Size markers are indicated on the left in kilodaltons. **(B)** GTP binding properties of ARF6 and ARF6 mutants. A nitrocellulose membrane was prepared as described above and assayed for binding to [<sup>32</sup>P]GTP as described (25), and the bound radioactivity was visualized by autoradiography.

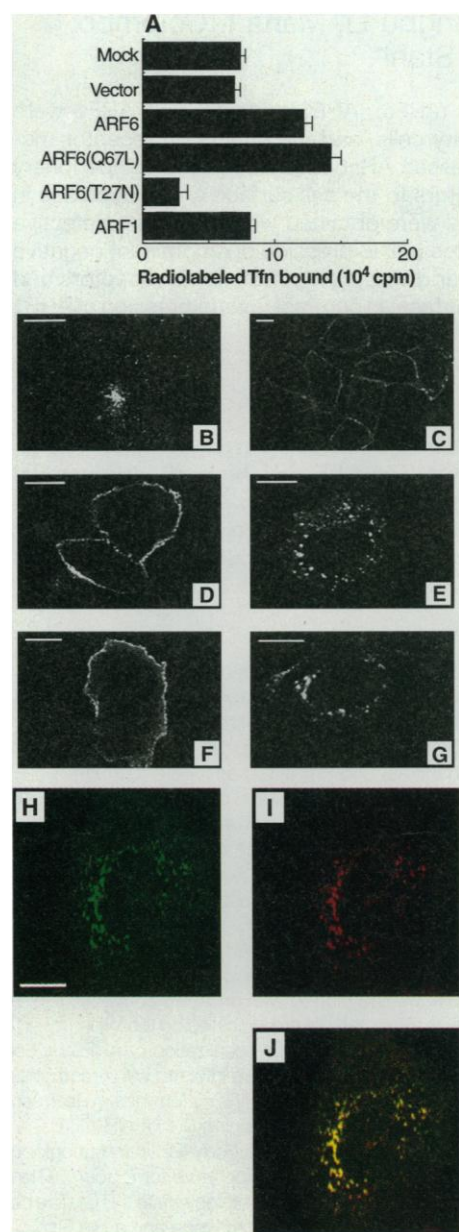
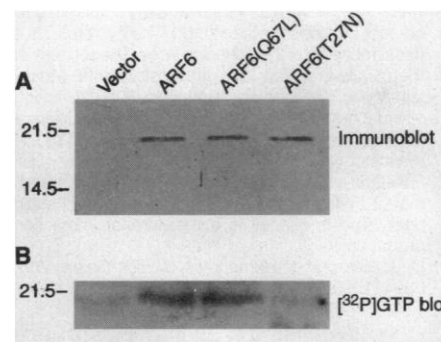


**Fig. 3. (A)** Cell surface distribution of Tfn-Rs. TRVb-1 cells were infected with the vector virus as a negative control or with recombinant virus expressing either ARF6, ARF6(Q67L), ARF6(T27N), or ARF1. At 4 hours after viral infection, the cell surface distribution of the Tfn-Rs was monitored as described (22). Each infection was done in triplicate, and the standard deviation is shown. **(B)** through **(G)** Localization of Tfn-Rs and ARF6 mutants by confocal immunofluorescence microscopy. TRVb-1 cells grown on cover slips were infected with either the vector virus as a negative control (B) or with recombinant virus expressing ARF6 (C), ARF6(Q67L) (D and F), and ARF6(T27N) (E and G). At 5 hours after infection, cells were fixed and permeabilized as described for Fig. 2B. Cells were incubated with a monoclonal antibody, B3/25, against the human Tfn-R (Boehringer Mannheim) (B, C, D, and E) or with affinity-purified ARF6 antibody (F and G) and stained with a goat antibody to mouse IgG (B, C, D, and E) or goat antibody to rabbit IgG (F and G) coupled to FITC (Sigma). Cover slips were mounted in 1% propyl gallate and viewed with a Zeiss axiovert microscope and a Bio-Rad confocal scanning imaging system. Bars = 10  $\mu$ m. **(H)** through **(J)** Colocalization of ARF6(T27N) and Tfn-Rs by double immunofluorescence labeling. TRVb-1 cells (on cover slips) expressing ARF6(T27N) were treated as described above, except that the cells were incubated with both primary antibodies, the affinity-purified ARF6 antibody (H) and B3/25 (I), and stained with goat antibody to rabbit IgG coupled to FITC and donkey antibody to mouse IgG coupled to Cy-3 (Chemicon), respectively. To visualize the degree of colocalization of ARF6 and Tfn-Rs, we merged the two confocal images. Colocalization was indicated when coincident red and green staining appeared yellow (J). Bar = 10  $\mu$ m.

tracellular compartments (Fig. 3). These compartments varied in size and ranged from large vesicular aggregates to smaller, more punctate structures. The intracellular localization of the ARF6 mutants was then examined with the use of the affinity-purified ARF6 antibody. The distribution pattern of the ARF6 mutants appeared to match that described above for the Tfn-Rs in the mutant transfectants. Mutant ARF6(Q67L) was predominantly localized to the plasma membrane, whereas the distribution of the ARF6(T27N) mutant was shifted to intracellular structures (Fig. 3). Double labeling

experiments in cells transfected with ARF6(T27N) revealed an almost identical intracellular staining pattern for Tfn-Rs and ARF6(T27N) (Fig. 3).

Next, we monitored the kinetics of Tfn internalization and release during a single cycle of Tfn transport. Iron-loaded [<sup>125</sup>I]Tfn was bound to cells at 4°C, excess ligand was removed, and the cells were rapidly warmed to 37°C in medium containing unlabeled Tfn (100-fold excess). At various times thereafter, the amounts of [<sup>125</sup>I]Tfn released into the medium were determined. The rate of [<sup>125</sup>I]Tfn release from cells overexpressing ARF6, ARF6(Q67L), or ARF6(T27N) was decreased significantly compared to that in the cells infected with the vector virus or in the cells infected with the recombinant virus overexpressing ARF1 (Fig. 4). Following a similar time course, we monitored cell surface [<sup>125</sup>I]Tfn by washing the cells with a low pH buffer (Fig. 4B). Although the rate of decrease in cell surface Tfn was similar in cells infected with the vector virus and in cells overexpressing ARF1, the rate was greatly reduced in cells overexpressing ARF6 or ARF6(Q67L), suggesting that overexpression of these proteins inhibited internalization of Tfn. Overexpression of ARF6(T27N) resulted in only a slight decrease in the internalization rate of Tfn (Fig. 4). In control cells infected with vector virus and in cells overexpressing ARF1, approximately 60% of prebound Tfn transiently accumulated within the cell after a 2.5-min incubation, followed by a rapid decrease of cell-associated Tfn, reflecting the recycling of Tfn into the medium (Fig. 4). This transient intracellular accumulation of Tfn was delayed in cells overexpressing ARF6 or ARF6(Q67L) but was eventually recycled into the medium (Fig. 4). In contrast, overexpression of ARF6(T27N) caused a prolonged intracellular accumulation of Tfn with 50% of the ligand still found within the cells after 30 min of incubation at 37°C. This suggests that expression of ARF6(T27N) dramatically decreased the recycling rate, and as a consequence the internalized Tfn was trapped within the cells. These observations on the kinetics of Tfn recycling agree with the Tfn distribution data (Fig. 3).

In summary, our data show that overexpression of ARF6 but not of ARF1 produces dramatic changes in endocytic traffic. Overexpression of ARF1(Q71L) [a mutant form of ARF1 that is defective in GTP hydrolysis and that localizes to the Golgi apparatus (4)] decreases fluid phase endocytosis but profoundly alters Golgi morphology without causing morphological changes in endosomes (12). Furthermore, overexpression of ARF1(Q71L) causes no significant changes in Tfn-R uptake and recycling (13). Thus, ARF1(Q71L) may inhibit fluid phase endocytosis indirectly by

inhibiting the delivery of recycling membrane from the Golgi apparatus to the plasma membrane, which is required for prolonged endocytosis. The colocalization of Tfn-R and the ARF6 mutants suggests not only that ARF6 is an integral part of the endocytic machinery, but that its GTP cycle and its nucleotide status regulate progression through the endocytic pathway. One hypothesis for the site of action of ARF6 is at early endosomes where ARF6 could promote budding and the formation of transport vesicles. A  $\beta$ -COP-like protein has been identified on highly purified phagosome (14) and endosome (15) fractions, indicating the potential for transport vesicle formation from early endosomes. Thus, overexpression of the dominant negative mutant ARF6(T27N) may block budding from an early endosomal compartment and, as a result, reduce recycling to the cell surface. Alternatively, overexpression of ARF6 or of ARF6(Q67L), the activated form of the protein, may enhance budding from early endosomes, resulting in a fragmentation of the endosomal apparatus, a phenomenon reminiscent of Golgi stack fragmentation with continued COP-coated vesicle budding (16). This may explain the predominant cell surface distribution of Tfn-Rs upon expression of ARF6 and ARF6(Q67L). Alternative explanations [including a direct effect of ARF6 and ARF6(Q67L) on the plasma membrane blocking internalization] cannot be ruled out. Nevertheless, our studies indicate a fundamental role for ARF6 in endocytosis.

REFERENCES AND NOTES

1. R. A. Kahn and A. G. Gilman, *J. Biol. Chem.* **259**, 6228 (1984); *ibid.* **261**, 7906 (1986).
2. J. Clark *et al.*, *Proc. Natl. Acad. Sci. U.S.A.* **90**, 8952 (1993); A. Schurmann *et al.*, *J. Biol. Chem.* **269**, 15683 (1994).
3. M. Tsuchiya *et al.*, *J. Biol. Chem.* **266**, 2772 (1991).
4. S. B. Teal, V. W. Hsu, P. J. Peters, R. D. Klausner, J. G. Donaldson, *ibid.* **269**, 3135 (1994).
5. J. G. Donaldson, D. Cassel, R. A. Kahn, R. D. Klausner, *Proc. Natl. Acad. Sci. U.S.A.* **89**, 66408 (1992); D. J. Palmer, J. B. Helms, J. M. Beckers, L. Orci, J. E. Rothman, *J. Biol. Chem.* **268**, 12083 (1993); L. M. Traub, J. A. Ostrum, S. Kornfeld, *J. Cell Biol.* **123**, 561 (1993); M. A. Stamnes and J. E. Rothman, *Cell* **73**, 999 (1993); R. A. Kahn *et al.*, *J. Biol. Chem.* **267**, 10339 (1992).
6. W. E. Balch, R. A. Kahn, R. Schwaninger, *J. Biol. Chem.* **267**, 13053 (1992).
7. A. L. Boman, T. C. Taylor, P. Melançon, K. L. Wilson, *Nature* **358**, 512 (1992).
8. J. M. Lenhard, R. A. Kahn, P. D. Stahl, *J. Biol. Chem.* **267**, 13047 (1992).
9. T. E. McGraw, L. Greenfield, F. R. Maxfield, *J. Cell Biol.* **105**, 207 (1987).
10. All DNA manipulations were conducted according to standard methods (17). In order to insert the complementary DNA (cDNA) sequence of ARF6 or ARF1 into the Xba I site of the Sindbis vector pTotol0003'2J (18), the ARF cDNA sequences were amplified from Bluescript-ARF6 and POW12-ARF1 plasmids by 25 cycles of the polymerase chain reaction. The primers for ARF6 were 5'-GCTCTA-GAATTGGGGGAGGTGCTACCC-3' and 5'-GCTCT-AGATTAAAGATTGTAGTTAGAGG-3', which con-

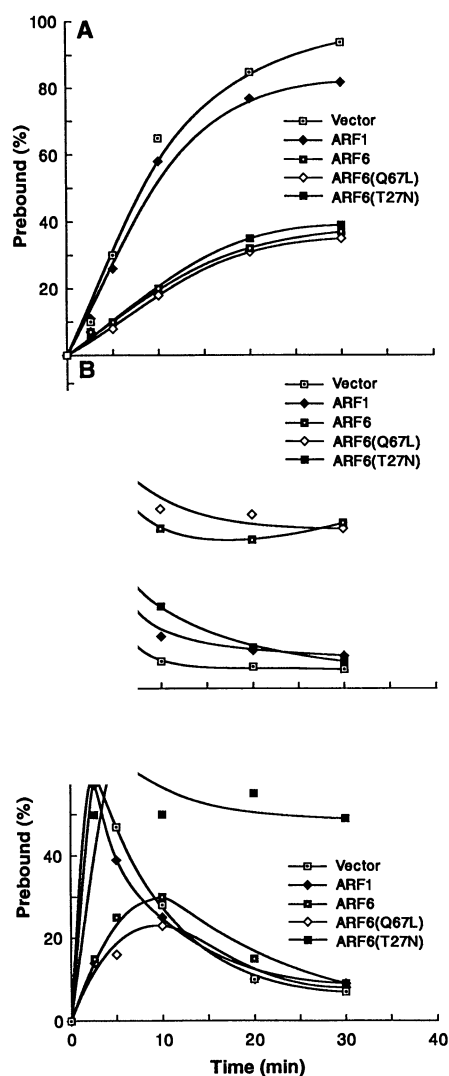


**Fig. 4.** Kinetics of Tfn recycling in TRVb-1 cells overexpressing ARF6, ARF6(Q67L), ARF6(T27N), and ARF1. After depletion of endogenous Tfn, cells were incubated with [<sup>125</sup>I]Tfn at 4°C (22). After removal of unbound ligand, cells were allowed to internalize prebound [<sup>125</sup>I]Tfn by rapid warming to 37°C (26). At the indicated time points, the medium was collected and radioactivity determined (recycled Tfn) (A); the cells were stripped of surface radioactivity by acid washes (surface-bound Tfn) (B); and finally, the cells were lysed, and cell-associated radioactivity was measured (intracellular Tfn) (C).

tained the Xba I linker followed by sequences corresponding to the NH<sub>2</sub>- and COOH-terminal sequences of ARF6, respectively. ARF1 cDNA was amplified with primers 5'-GCTCTAGAATGGGGAACATCTTCGCG-3' and 5'-GCTCTAGACTACTTCTGGT-TCCGGAGC-3', which contained the Xba I linker followed by NH<sub>2</sub>-terminal and COOH-terminal sequences of ARF1, respectively. The amplified ARF cDNAs were digested with the restriction endonuclease Xba I (Life Technologies), followed by ligation into the Xba I site of pTotol0003'2J, which was previously linearized by Xba I digestion and treated with calf alkaline phosphatase. The correct sequence and orientation of the insert were confirmed by DNA sequencing. The pTotol0003'2J-ARF constructs were used for recombinant virus production as described (18). The recombinant viruses were called SIN:ARF6 and SIN:ARF1 and were stored in aliquots at -70°C and were thawed just before use. The virus stock derived from the Sindbis vector pTotol0003'2J (SIN) served as a negative control for the described experiments. The substitution mutations ARF6(T27N) and ARF6(Q67L) were created by oligonucleotide-directed mutagenesis with use of the Bio-Rad phagemid mutagenesis system that was based on Kunkel's method of mutagenesis (19). The cDNA sequences of ARF6 were cloned into the Xba I site of the pGC2 plasmid (20) as described above for pTotol0003'2J. Because pGC2 contains the M13 phage replication origin, single-stranded DNA templates were produced with the use of the helper phage M13K07 and were used as templates for mutagenesis. The oligonucleotides 5'-GATCTT-GTCCAGGCCGCCACCATC-3' and 5'-GTACAG-GATTGTGT TCTTGCCGCGCG-3' were used to generate mutations ARF6(Q67L) and ARF6(T27N), respectively. The mutations were verified by DNA sequencing. The amplified mutant cDNAs were digested with Xba I and inserted into the Sindbis vector pTotol0003'2J. The plasmids were subsequently used for recombinant virus production as described above.

11. C. D'Souza-Schorey, G. Li, M. I. Colombo, P. D. Stahl, data not shown.
12. C. Zhang *et al.*, *J. Cell Biol.* **124**, 289 (1993).
13. C. D'Souza-Schorey and P. D. Stahl, unpublished results.
14. W. Beron, M. I. Colombo, C. D'Souza-Schorey, P. D. Stahl, unpublished results.
15. J. A. Whitney, T. E. Kreis, I. Mellman, *Mol. Biol. Cell.* **4**, 445a (1993).
16. T. Mistelli and G. Warren, *J. Cell Biol.* **125**, 269 (1994).
17. J. Sambrook, E. F. Fritsch, T. Maniatis, in *Molecular Cloning: A Laboratory Manual* (Cold Spring Harbor Laboratory, Cold Spring Harbor, NY, 1989).
18. G. Li and P. D. Stahl, *J. Biol. Chem.* **268**, 24475 (1993).
19. T. A. Kunkel, *Proc. Natl. Acad. Sci. U.S.A.* **82**, 488 (1985).
20. R. M. Myers, L. S. Lerman, T. Maniatis, *Science* **229**, 242 (1985).
21. P. D. Stahl *et al.*, *Cell* **19**, 207 (1980).
22. To determine cell surface distribution of Tfn-Rs, we incubated cells with serum-free Ham's F-12 media (pH 7.4) containing 0.2% bovine serum albumin (BSA) for 1 hour to deplete cells of endogenous Tfn. Iron-loaded human Tfn was labeled with <sup>125</sup>I as described (21). Binding of [<sup>125</sup>I]Tfn to the cell surface was conducted at 4°C for 90 min in serum-free Ham's F-12 media (pH 7.4) containing 0.2% BSA and a saturating concentration of [<sup>125</sup>I]Tfn (6 μg/ml). Unbound Tfn was removed by four washes with phosphate-buffered saline (PBS) containing 0.2% BSA. Cells were scraped from the dishes and counted for radioactivity. Nonspecific binding was determined by including unlabeled Tfn (100-fold excess) and accounted for <10% of the total Tfn bound.
23. A 12-amino acid peptide, CKLTWLTNSKYS, close to the COOH-terminal end of ARF6 was coupled to rabbit serum albumin (RSA) and injected into rabbits for polyclonal antibody production (Cocalcol Biologicals). Abbreviations for the amino acid residues are C, Cys; K, Lys; L, Leu; N, Asn; S, Ser; T, Thr; W, Trp; and Y, Tyr. The antiserum generated was purified by sequential chromatography on columns of activated

CNBr-sepharose 4B (Pharmacia) coupled to the ARF6 peptide-RSA conjugate and protein A sepharose (Sigma).

24. Viral infection was conducted at a multiplicity of infection of 50 plaque-forming units per cell in 200 μl of PBS containing 1% fetal bovine serum (FBS). Virus adsorption was conducted at 4°C for 1 hour. The infection mixtures were replaced by 3 ml of Ham's F-12 medium (Gibco-BRL), supplemented with 5% FBS (Hyclone) and incubated at 37°C for the appropriate time periods as indicated (18). More than 90% of the cells were infected when the infections were done on plastic 35-mm tissue culture dishes. When infections were done on glass cover slips, 40 to 65% of the cell population was infected.
25. P. Wagner, L. Hengst, D. G. Gallwitz, *Methods Enzymol.* **219**, 369 (1992).
26. After depletion of endogenous Tfn, binding of [<sup>125</sup>I]Tfn to the cell surface was conducted as described (22); this was followed by four washes with PBS to remove unbound ligand. The uptake was initiated by adding prewarmed Ham's F-12 medium (pH 7.4) containing 0.2% BSA and a 100-fold excess of cold Tfn, and cells were incubated at 37°C for different times as indicated in Fig. 4. At each time point the medium was collected and the cell monolayers were washed once with PBS containing 0.2% BSA. The medium and the wash were combined and the radioactivity was determined (recycled Tfn). The concentration of cell surface-bound [<sup>125</sup>I]Tfn was determined by acid strip-

ping. Cell monolayers were washed twice with ice-cold 0.5% acetic acid and 0.5 M NaCl (pH 3.0), followed by one wash with PBS. The washes were pooled and measured for radioactivity (surface-bound Tfn). Finally, the cells were solubilized with PBS containing 1% Triton X-100 and 0.1% NaOH, and the radioactivity in the lysates was determined (intracellular Tfn). More than 90% of the radioactivity released was precipitable by trichloroacetic acid.

27. We thank R. Klausner and P. Peters (NIH) for sharing data before publication, for helpful comments, and for BL21 cells expressing ARF proteins; M. Vaughan and J. Moss (NIH) for the ARF6 cDNA; C. Rice (Washington University) for the pTotol0003'2J plasmid; T. McGraw (Columbia University) for the TRVb-1 cell line; J. Rothman (Memorial Sloan Kettering Cancer Center) for antibody to recombinant ARF1; J. Heuser (Washington University) for helpful suggestions and for critical reading of the manuscript; M. Linder and L. Mayorga for critical reading of the manuscript; D. Schafer and S. Pontow for assistance with confocal microscopy; and R. L. Boshans and L. LaRose for excellent technical assistance. C.D.S. is a Lucille P. Markey postdoctoral fellow, G.L. is a fellow of the Parker B. Francis Foundation, and M.I.C. is supported by the Leukemia Society of America. This work was supported in part by NIH grants to P.D.S.

23 November 1994; accepted 20 January 1995

## DNA-Dependent Kinase (p350) as a Candidate Gene for the Murine SCID Defect

Cordula U. Kirchgessner, Christopher K. Patil, James W. Evans, Christina A. Cuomo, Laura M. Fried, Timothy Carter, Marjorie A. Oettinger, J. Martin Brown\*

Severe combined immunodeficient (SCID) mice are deficient in a recombination process utilized in both DNA double-strand break repair and in V(D)J recombination. The phenotype of these mice involves both cellular hypersensitivity to ionizing radiation and a lack of B and T cell immunity. The catalytic subunit of DNA-dependent protein kinase, p350, was identified as a strong candidate for the murine gene *SCID*. Both p350 and a gene complementing the SCID defect colocalize to human chromosome 8q11. Chromosomal fragments expressing p350 complement the SCID phenotype, and p350 protein levels are greatly reduced in cells derived from SCID mice compared to cells from wild-type mice.

DNA repair systems are essential in maintaining the structural integrity of genes. Unrepaired DNA damage may result in far-reaching consequences such as mutagenesis, genomic instability, tumorigenesis, and cell death. Cells have evolved distinct DNA repair pathways to cope with particular DNA lesions, and most of these pathways show conservation between lower and higher eukaryotes, such as between yeast and humans. However, DNA double-strand breaks, which confer the highest potential

for genomic instability and cell death, appear to be repaired in mammalian cells by a unique pathway. The mouse mutant SCID (1) is the only known animal model with a deficiency in this recombination pathway. This pathway functions in V(D)J recombination, the process of assembling the immunoglobulin and T cell receptor genes from gene segments by site-specific recombination, and in DNA repair. The SCID defect in immature lymphocytes appears to be in one of the final steps of V(D)J recombination, the joining of the free DNA ends of the coding strands, whereas joining of the recombination signal sequences is relatively normal (2). SCID mice lack both B and T cell immunity as the result of their deficiency in V(D)J recombination, and are sensitive to ionizing radiation in all cell types, because of their deficiency in DNA double-strand break repair (3).

C. U. Kirchgessner, C. K. Patil, J. W. Evans, L. M. Fried, J. M. Brown, Department of Radiation Oncology, Stanford University School of Medicine, Stanford, CA 94305, USA.

C. A. Cuomo and M. A. Oettinger, Department of Molecular Biology, Massachusetts General Hospital, Boston, MA 02114, USA.

T. Carter, Department of Biological Sciences, St. John's University, Jamaica, NY 11439, USA.

\*To whom correspondence should be addressed.